Environmental Science and Pollution Research (2019) 26:26869–26882
https://doi.org/10.1007/s11356-019-05931-3

RESEARCH ARTICLE

Effects of different scrap iron as anode in Fe-C micro-electrolysis system for textile wastewater degradation

Zhenhua Sun[1] · Zhihua Xu[1] · Yuwei Zhou[1] · Daofang Zhang[1] · Weifang Chen[1]

Received: 5 April 2019 / Accepted: 8 July 2019 / Published online: 13 July 2019

Abstract

The degradation of organic contaminants in actual textile wastewater was carried out by iron carbon (Fe-C) micro-electrolysis. Different Fe-C micro-electrolysis systems (SIPA and SISA) were established by using scrap iron particle (SIP) and scrap iron shaving (SIS) as anode materials. The optimal condition of both systems was obtained at the initial pH of 3.0, dosage of 30 g/L and Fe/C mass ratio of 1:1. Commercial spherical Fe-C micro-electrolysis material (SFC) was used for comparison under the same condition. The results indicated that total organic carbon (TOC) and chroma removal efficiencies of SIPA and SISA were superior to that of SFC. Total iron concentration in solution and XRD analysis of electrode materials revealed that the former showed relatively high iron corrosion intensity and the physicochemical properties of scrap iron indeed affected the treatment capability. The UV-vis and 3DEEM analysis suggested that the pollutants degradation was mainly attributed to the combination of reduction and oxidation. Furthermore, the potential degradation pathways of actual textile wastewater were illustrated through the GC-MS analysis. Massive dyes, aliphatic acids, and textile auxiliaries were effectively degraded, and the SIPA and SISA exhibited higher performance on the degradation of benzene ring and dechlorination than that by SFC. In addition, SIPA and SISA exhibited high stability and excellent reusability at low cost.

Keywords Fe-C micro-electrolysis · Textile wastewater · Scrap iron · Effluent organic matter · Degradation pathway · Reduction and oxidation

Introduction

With the rapid development of textile industry, wastewater discharged during the textile processing has been increasing. It was reported that around 40 to 65 L of wastewater was generated per kg of textile produced (Manu and Chaudhari 2002). The wastewater contained various industrial chemicals, such as dyes, finishing agents, surfactants, dispersants, emulsifiers and salts, on account of their excessive use during the complex and lengthy textile processing (Khandegar and Saroha 2013). And the overwhelming majority of these chemicals were toxic, hazardous, and refractory. The amount of residue was inevitably released into environment through effluents, posing adverse effects on aquatic ecosystem and human health. Besides, dyes created esthetic pollution due to their high visibility even in low concentrations (Brillas and Martínez-Huitle 2015). Hence, the elimination of contaminants and decolorization treatment of textile wastewater have been intensively investigated in the past few decades.

Although biological technology was the cheapest and most widely used industrial wastewater treatment methods, it exhibited limited removal efficiency for the high toxicity and biologically stability of textile wastewater. Therefore, different synergistic treatment techniques have been explored to remove the negative impacts of textile wastewater on microorganism such as adsorption

Zhenhua Sun and Zhihua Xu contributed equally to this work.

Highlights
- Different scrap irons were used as anode materials to construct Fe-C micro-electrolysis systems for actual textile wastewater degradation.
- The effects of the physicochemical properties of scrap iron itself on TOC removal efficiency were discussed.
- Degradation pathways of organic pollutants in textile wastewater based on Fe-C micro-electrolysis systems were illustrated.

Responsible editor: Bingcai Pan

✉ Zhihua Xu
zhihuaxu_usst@126.com

[1] School of Environment and Architecture, University of Shanghai for Science and Technology, 516 Jungong Rd., Shanghai 200093, People's Republic of China

(Regti et al. 2016), electrochemistry (Yahiaoui et al. 2013), photocatalysis (Li et al. 2017), Fenton (Doumic et al. 2015), and ozonation (Eremektar et al. 2007). Adsorption could separate the contaminants from solution but hardly degrade them, which was unfavorable to improve the biodegradability of textile wastewater. Electrochemistry and photocatalysis could eliminate pollutants effectively; however, the processes were highly specific conditions-dependent. Fenton and ozonation showed potential to degrade organic pollutants, but the high costs rendered them difficult to be widely applied. Thus, it is eagerly demanded to develop a more economically feasible method for textile wastewater treatment. Recently, as a promising technology for refractory wastewater degradation, iron carbon (Fe-C) micro-electrolysis has attracted extensive attention due to its low cost, simple operation and high treatment efficiency (Lai et al. 2013; Yang et al. 2017b). In Fe-C micro-electrolysis, Fe^0 and activated carbon (AC) were commonly used as electrode materials, forming numerous microscopic galvanic cells spontaneously by the direct contact and mixture. Fe^0 as anode provided the electrons and released Fe^{2+} simultaneously, while AC acted as cathode to accept and transfer the electrons to solution. Under anoxic conditions, the electrons, [H] and Fe^{2+} generated in the system possessed excellent activity to reduce organic pollutants via reduction reactions (Lai et al. 2012; Van der Zee et al. 2003). Moreover, Fe^{2+} could be converted into iron hydroxides flocs and then remove pollutants by coagulation and precipitation (Ying et al. 2012). Under aerobic conditions, dissolved oxygen accepted electrons to generate H_2O_2, which could further form ·OH and Fenton-like reaction in the presence of Fe^{2+}, presenting an excellent organic pollutants mineralization effect (Deng et al. 2018; Ruan et al. 2010). The main reactions involved in Fe-C micro-electrolysis could be represented as follows:

Iron anode (oxidative):

$$Fe^0 - 2e^- \rightarrow Fe^{2+} \quad (1)$$

$$Fe^{2+} - e^- \rightarrow Fe^{3+} \quad (2)$$

Carbon cathode (reductive):

$$2H^+ + 2e^- \rightarrow [H] \rightarrow H_2 \quad (3)$$

$$H_2O + e^- \rightarrow [H] + OH^- \quad (4)$$

Acidic with oxygen:

$$O_2 + 2H^+ + 2e^- \rightarrow H_2O_2 \quad (5)$$

$$Fe^{2+} + H_2O_2 \rightarrow Fe^{3+} + \cdot OH + OH^- \quad (6)$$

Electro-coagulation:

$$Fe^{2+} + OH^- \rightarrow Fe(OH)_2 \rightarrow Fe(OH)_3 \quad (7)$$

Some previous studies on the anode material of Fe-C micro-electrolysis were focused on the use of iron powder, which has high surface area and reactivity (Dou et al. 2010; Liu et al. 2016; Zhou et al. 2013). But the inherent properties like easy agglomeration and passivation of iron powder might restrict its application (Guan et al. 2015). To overcome these drawbacks, it was feasibly accepted to use scrap iron as a promising substitute anode material for iron powder for the construction of Fe-C micro-electrolysis. On the one hand, scrap iron possessed abundant production, relatively low cost and excellent hydraulic characteristic that could continuously provide electrons in solution with good mass transfer efficiency (Ou et al. 2016). On the other hand, environmental pollution and land resource occupation could be decreased simultaneously by reusing scrap iron as anode material, because scrap iron was a solid waste generated from the drilling and turning processes in iron and steel industries (Ya et al. 2018). Currently, considerable research efforts have been carried out on the effects of operation parameters on the treatment efficiency of Fe-C micro-electrolysis composed of scrap iron and AC (Han et al. 2016; Qin et al. 2012; Yang et al. 2017b). Nevertheless, the intrinsic physicochemical properties of electrode materials might also be a non-negligible factor. For cathode materials, Zhu et al. (Zhu et al. 2018a) found that the particle size, shape, and material species of AC had great influences on the treatment capability for Fe-C micro-electrolysis. While for anode materials, it was reported that the shape, size, surface area, and elemental composition of scrap iron affected its reactive activity, but little attention has been devoted to investigating its roles in subsequent formation of microscopic galvanic cells in Fe-C micro-electrolysis system (Btatkeu et al. 2013; Gheju and Balcu 2010). It was accordingly presumed that the treatment capability of Fe-C micro-electrolysis could be further affected by the physicochemical properties of scrap iron.

Consequently, in the present study, different scrap iron-AC micro-electrolysis systems were applied in actual textile wastewater treatment. The effects of physicochemical properties of scrap iron on the performance of micro-electrolysis system were investigated. Batch experiments were carried out to analyze the effects of key operational parameters on the treatment efficiency of textile wastewater. Additionally, the treatment efficiency and economic feasibility of scrap iron-AC systems were reasonably evaluated by comprehensive comparison of commercial Fe-C micro-electrolysis. Finally, the variations and possible degradation pathways with organic pollutant species in actual

textile wastewater were elucidated. The stability and cost analysis of different Fe-C micro-electrolysis systems was also investigated.

Materials and methods

Materials and reagents

Scrap iron particles (SIP) and scrap iron shavings (SIS) used in this study were supplied by a mechanical processing plant in Shanghai, P.R. China. The particle size of SIP and SIS were 1–3 mm and 5–8 mm, respectively. The commercial spherical Fe-C material (SFC) with a porous structure was purchased from Longantai Environmental Protection Co. in Zhejiang Province, P.R. China. The main chemical composition of SIP, SIS, and SFC were presented in Table 1. Before use, SIP, SIS, and SFC particles were soaked in 5% sodium hydroxide solution for 2 h to remove surface oxide layer and grease, then dipped into 5% hydrochloric acid solution for 20 min to further remove surface oxidation, and finally rinsed with deionized water until a neutral pH value was reached. Activated carbon (AC) (diameter 0.5–1 mm) was obtained from Sinopharm Chemical Reagent Co. in Shanghai, P.R. China. Before each experiment, AC was cleaned by tap water, and then soaked in the textile wastewater for 48 h to eliminate the effect of adsorption. Actual textile wastewater samples were obtained from the industrial effluent of Yashuai Textile Co., Ltd. in Zhejiang Province, P.R. China. The samples were immediately preserved at 4 °C to minimize biological and chemical reactions, and its general characteristics were TOC of 1214 ± 24 mg/L, chroma of 625 ± 35 times and pH of 7.15 ± 0.4. Hydrochloric acid (HCl) and sodium hydroxide (NaOH) were obtained from Sinopharm Chemical Reagent Co. in Shanghai, P.R. China, which were analytical grade and used without further purification. Deionized water prepared by Milli-Q Advantage A10 was used throughout the whole experiment process.

Experimental procedures

SIP and SIS were combined with AC to build SIPA and SISA micro-electrolysis systems, respectively. Batch experiments were conducted to determine the treatment capacity of both systems. The pH of the textile wastewater was adjusted using HCl (1 mol/L) and NaOH (1 mol/L). In each batch experiment, 200 mL actual textile wastewater and the desired dosage of Fe^0 and AC were added in a 500-mL flat bottom beaker, and the slurry was mixed by a mechanical stirrer at 200 rpm and room temperature throughout the experiment. The key effect factors, such as initial pH (1.0–9.0), Fe^0 and AC dosage (10–50 g/L) and Fe/C mass ratio (1:3–3:1), were investigated thoroughly. Samples were taken from the suspensions after 120 min treatment and then filtered through a 0.45-μm syringe membrane filter for analysis. In order to compare the treatment capacity of the above-mentioned systems with that of SFC system under the same operating conditions (initial pH of 3.0, dosage of 30 g/L, Fe/AC ratio of 1:1 and the stirring speed of 200 rpm), approximately 4 mL samples were taken from the suspensions at certain time intervals during the 180 min treatment period, and then filtered through a 0.45 μm syringe membrane filter for analysis. The experiments of TOC and chroma removal were conducted in triplicate, and then the average value was given. The mean deviation of 4.2% was observed in the reported data. In consecutive experiments, after each cycle, the electrode materials were washed with deionized water and dried for reuse.

Table 1 Main chemical composition of SIP, SIS, and SFC

Materials	Fe (%)	C (%)	Ca (%)	Cr (%)	Cu (%)	Mg (%)	Mn (%)
SIP	98.695	–	0.691	–	0.019	0.090	0.502
SIS	97.778	–	0.561	0.918	–	0.098	0.643
SFC	80.860	16.597	1.275	0.216	0.109	0.231	0.712

Analytical methods

Total organic carbon (TOC) of the samples was measured by a TOC meter (Analytikjena, multi N/C3100, Germany). The chroma was determined according to the national standard methods of P.R. China (GB11903-89). The total iron concentration was performed with an inductively coupled plasma (ICP-MS) analysis (PE, Optima 8000, USA). The phase compositions of electrode materials were performed by X-ray diffraction (XRD, Bruker D8 Advance, Germany) with Cu Kα radiation and recorded from 5 to 80° (2θ) at a scanning rate of 3°/min. The UV-vis absorption spectra analysis of the aqueous solutions were carried out in 10 mm quartz cuvettes and monitored by a UV-vis spectrophotometer (Shimadzu, UV 2600, Japan). The three-dimensional excitation-emission matrix fluorescence (3DEEM) was determined using a fluorimeter (Hitachi, F-7000, Japan). The organic species were analyzed using gas chromatography-mass spectrometry (GC-MS) (Agilent 7890A 5975C, USA) equipped with a Chrompack capillary column (DB-5MS, 0.25 μm × 30 m × 0.25 mm, Agilent) and an autosampler (Model 7683B Series Injector, Agilent) assembly. The program of the GC-MS was as follows: 0.4 μL sample was injected with an inlet temperature of 250 °C. Helium was the carrying gas with a gas flow rate of 45 cm/s. The initial oven temperature was kept at 60 °C for 1 min, then linearly ramped to 180 °C at 15 °C·min^{-1}, followed by temperature increment to 280 °C at 5 °C·min^{-1}, and finally kept at 280 °C for 8 min. The mass spectra were set in scan mode from 50 to 500 *m*/*z*.

Results and discussion

Parameters optimization

Effect of initial pH As shown in Fig. 1a, the variations in terms of TOC and chroma removal efficiency with different initial pH were discussed. The TOC and chroma removal efficiency decreased gradually when pH rose from 1.0 to 7.0, suggesting that both micro-electrolysis systems were highly acid-promoted. The electron transfer enhanced with the increase of H^+ concentration in solution and therefore Fe^{2+} dissolution and [H]/·OH generation accelerated (Lai et al. 2014). Meanwhile, the iron oxides and hydroxides coating on Fe^0 surface could be continuously dissolved, exposing more reactive sites and facilitating the corrosion reaction. It was generally accepted that the electron transfer rate would be remarkably inhibited in alkaline solution, thus the TOC and chroma removal efficiency of SISA continued to decline when the initial pH was 9.0. In contrast, it could be observed that the pollutant removal efficiency by SIPA was even increased under the same condition. The results revealed that SIP possessed relatively large available iron surface area because of its small particle radius, which could provide sufficient Fe^{2+} and Fe^{3+} even in alkaline solution and further induce the formation of floc iron sludge to separate pollutants via coagulation and adsorption (Yang et al. 2017b). However, in neutral and alkaline solution, the biodegradability of wastewater could hardly be improved due to the barely decomposition of pollutants, and the large amount of iron-containing sludge increased the cost of sludge treatment as well (Lai et al. 2013). Additionally, although acidic conditions significantly improved the treatment efficiency of dyeing wastewater, the Fe^0 might be excessively corroded and quickly consumed. Meanwhile, it was reported that massive hydrogen generated and attached on the surface of Fe^0 in extreme acidic conditions (pH < 3.0), hindering the electrons and Fe^{2+} transfer (Han et al. 2016). Hence, pH was controlled at 3.0 as the optimum initial pH for the following experiments.

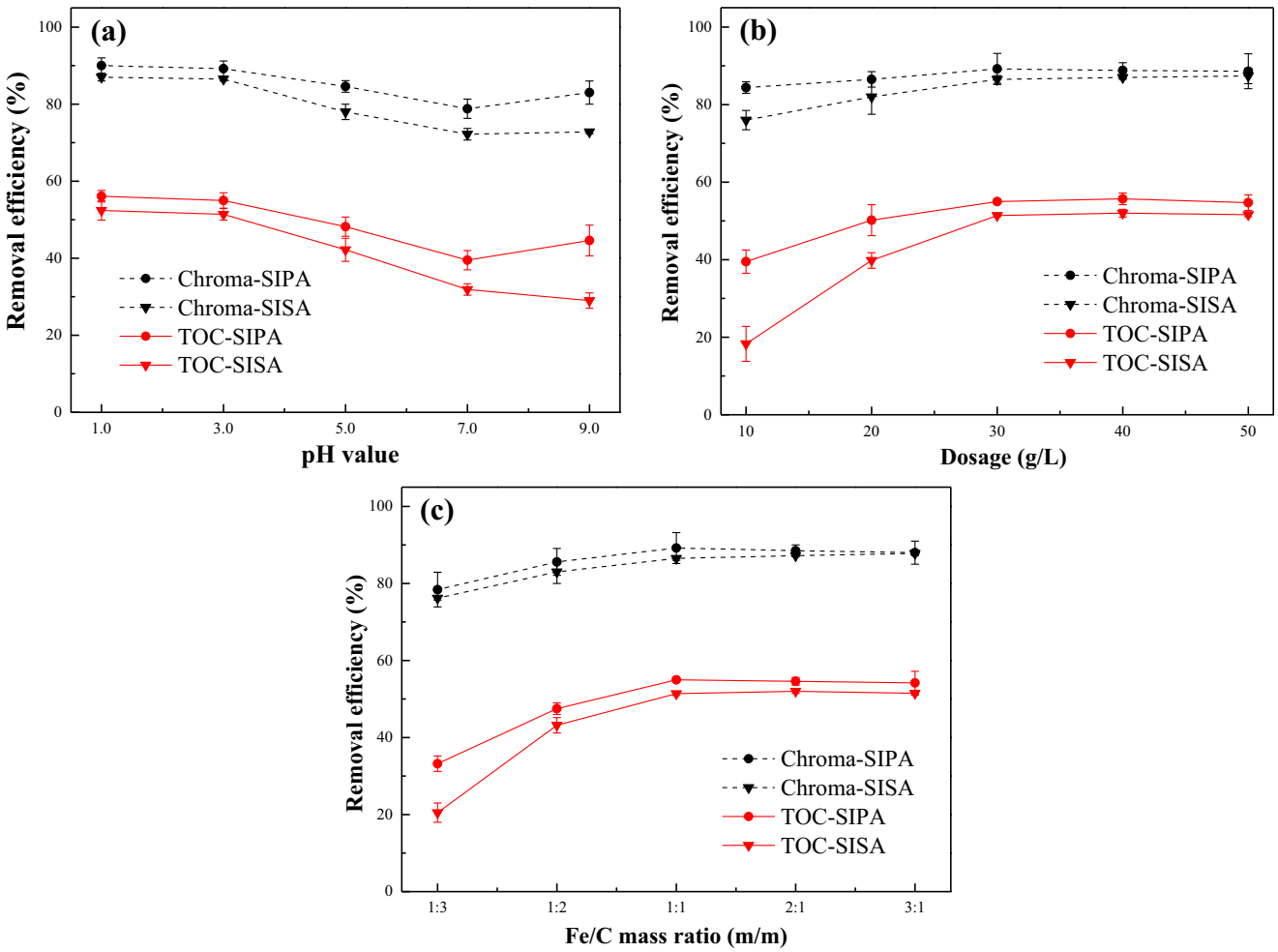

Fig. 1 Effect of **a** initial pH, **b** dosage, and **c** Fe/C mass ratio on the TOC and chroma removal efficiency. Experiment conditions: dosage = 30 g/L, Fe/AC ratio = 1:1, reaction time = 120 min, stirring speed = 200 rpm

Effect of dosage The effect of Fe^0 and AC dosage on TOC and chroma removal efficiency was evaluated by varying the dosages. As can be seen in Fig. 1b, the TOC and chroma removal efficiency treated by SIPA and SISA increased gradually when the dosage changed from 10 to 30 g/L, and the maximum promotion obtained when the dosage reached 30 g/L. This phenomenon could be explained by the increased available iron surface area, reactive sites as well as iron corrosion intensity when the dosage of Fe^0 increased (Lai et al. 2014). At the same time, SISA treatment had lower TOC and chroma removal efficiency compared with SIPA owing to smaller available iron surface area of SIS. Figure 1b also depicted that the removal efficiency of TOC and chroma was basically stable, even gradually declined, with further increasing of Fe^0 and AC dosage from 30 to 50 g/L, which could be attributed to the inhibition of mass transfer caused by excessive Fe^0 and AC. Considering the efficiency and the mass transfer resistance imposed by excessive Fe^0 and AC, 30 g/L dosage was selected as the optimal dosage for the subsequent experiments.

Effect of Fe/C mass ratio Fe^0 and AC were utilized as the anode and the cathode of micro-electrolysis system, respectively. In this system, Fe^0 provided electrons for the degradation of refractory and persistent organic contaminants in wastewater; meanwhile, the addition of AC was favor to forming a large number of microscopic galvanic cells by contacting scrap iron and significantly increased the treatment capacity (Lai et al. 2013; Liu et al. 2007). Therefore, the Fe/C mass ratio was an important parameter which could remarkably influence the degradation efficiency of organic pollutants. Figure 1c displayed the similar variations of SIPA and SISA in TOC and chroma removal efficiency with different Fe/C mass ratios from 1:3 to 3:1. As expected, it was found that increasing the Fe/C mass ratio from 1:3 to 1:1 greatly increased the TOC and chroma removal efficiency. Under the given total dosage of Fe^0 and AC, the more Fe^0 existed, the more Fe^{2+} dissolved, and thus the treatment efficiency of the micro-electrolysis system was apparently enhanced. Subsequently, the removal efficiency of TOC and chroma first kept steady then slightly decreased when the Fe/C mass ratio was above 1:1, indicating that the scarcity of AC was unfavorable to the formation of microscopic galvanic cells (Luo et al. 2014). According to previous studies, it was known that micro-electrolysis reactions and galvanic corrosion could be well facilitated when the Fe/C mass ratio was 1:1, because almost the same number of anode and cathode contributed to the formation of microscopic galvanic cells (Han et al. 2016; Liu et al. 2007). Accordingly, it could be concluded that Fe/C mass ratio that promoted TOC and chroma removal optimally in micro-electrolysis system was 1:1.

On the basis of spherical and porous structure, SFC as a commercial micro-electrolysis material provided big convenience for process operation by reducing pressure drop in flow-through systems and easily separation from treated water (Yuan et al. 2015). Hence, the treatment capability of SIPA and SISA systems for actual textile wastewater was compared simultaneously with that of SFC for further evaluation.

TOC and chroma removal efficiency

The variation of TOC and chroma removal efficiency over time at optimal parameters was depicted in Fig. 2. Obviously, the variation trend of chroma and TOC removal efficiency showed high relativity. The remove process could be divided into three parts. In the initial stage (0–20 min), the treatment effect of SFC was much better than SIPA and SISA, reasonably considering that the porous structure of the former material could rapidly adsorb the organic pollutants on its surface (Huang et al. 2014). While in the second stage (20–90 min), the growth of TOC and chroma removal efficiency of SFC gradually slowed down and was finally exceeded by SIPA and SISA. The result implied that the adsorption capacity of SFC material was limited, and large amount of pollutants on its surface made a heavy mass transfer resistance of electrons from Fe^0 to solution. Besides, the corrosion products of Fe^0 might hardly overcome the dense pollutant layer and also adhered to the SFC surface (Xu et al. 2016). For the latter two systems, the pollutants and corrosion products were mainly concentrated on AC surface as a consequence of outstanding porosity and hydrophobicity and the continuously released adsorption sites, contributing to reducing the surface load of Fe^0 and accelerating its corrosion. As time went on, the passivating layer coated on the Fe^0 surface, which was formed by iron oxides and hydroxides, noticeably hindering the electrons and Fe^{2+} transfer and the reactive activity of Fe^0. And the removal rate of TOC and chroma gradually decreased due to the scarcity of Fe^{2+}, [H], and ·OH. In the third stage (90–

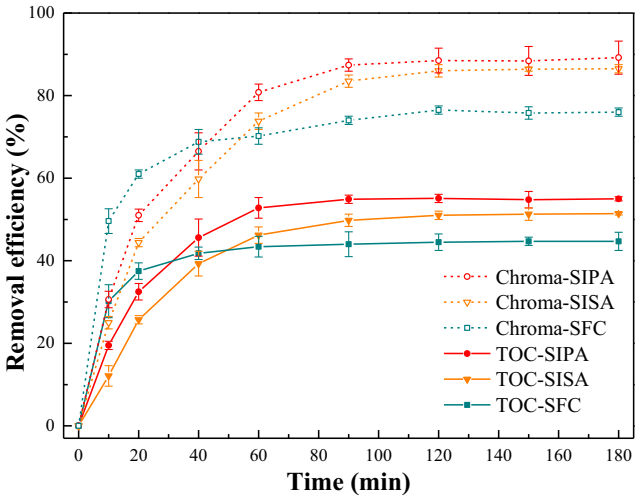

Fig. 2 Variation of the removal efficiency of TOC and chroma over time. Experiment conditions: initial pH = 3.0, dosage = 30 g/L, Fe/AC = 1:1, stirring speed = 200 rpm

180 min), the TOC and chroma removal efficiency remained stable, and the final results followed the sequence of SIPA > SISA > SFC. Both SIPA and SISA achieved more than 51% of TOC removal and 86.5% of chroma removal efficiency, which were much higher than that obtained by SFC. That is, the refractory organic pollutants in actual textile wastewater might be easier to degrade through a series of reduction reactions in SIPA and SISA.

Total iron concentration

It was well-known that the electrochemical corrosion of Fe^0 provided electrons to reduce pollutants, especially under acidic condition. Meanwhile, Fe^{2+} was generated and released into aqueous solution during the electron transfer process (Yamaguchi et al. 2018). The released iron in aqueous solution existed mainly as Fe^{2+}, and a small amount of Fe^{3+} could be reduced to Fe^{2+} in the presence of Fe^0 (Sun et al. 2016; Zhu et al. 2018b). Figure 3 illustrated the total iron concentration in aqueous solution after 120 min different micro-electrolysis treatments, it was observed that the total iron concentration in SIPA (1.690 mg/L) was higher than in SISA (1.529 mg/L), and SFC obtained the lowest total iron concentration (1.223 mg/L). The phenomenon could be explained by two aspects: (1) Larger available iron surface area of SIP than that of SIS resulted in higher iron corrosion reaction intensity and Fe^{2+} generation, thus promoting the formation of highly active [H] and ·OH. (2) With the same dosage, the theoretical iron proportion of SFC (80.86%) was much higher than that of SIPA (50%) and SISA (50%), whereas the released total iron was relatively low since the heavy mass transfer resistance caused by the layer of pollutants and corrosion products attached to the SFC surface. Obviously, the physicochemical properties of electrode materials highly affected the Fe^0 corrosion reaction, which was the dominant process to degrade organic pollutants.

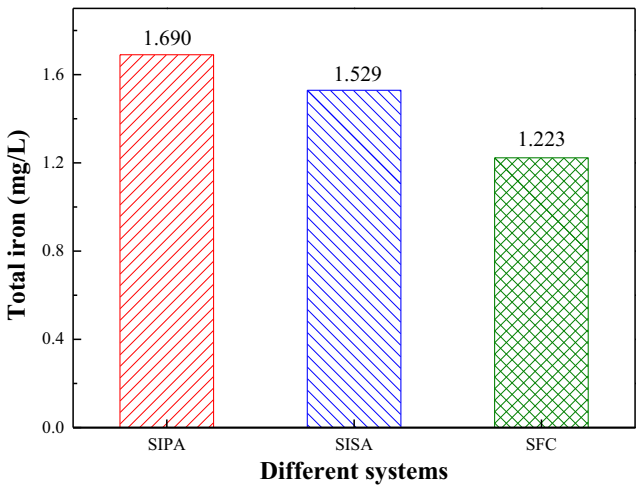

Fig. 3 Total iron concentration in solution after 120 min treated by different micro-electrolysis systems

XRD analysis

To confirm the chemical ingredients of different materials before and after micro-electrolysis treatment time of 120 min, the fresh and micro-electrolysis treated SIP, SIS, SFC, and AC were further analyzed by XRD. Figure 4a showed the XRD analysis of the chemical composition of the fresh SIP, SIS, and SFC, which were mainly Fe^0, and a small amount of Fe_3O_4 located at $2\theta = 36°$ was also detected in SFC (Xu et al. 2019, 2018b; Zhang et al. 2016). The Fe_3O_4 generation of SFC was likely attributed to the oxidation of iron during the preparation process under high temperature. After micro-electrolysis treatment, the intensity of peaks corresponding to Fe^0 in SIP, SIS, and SFC were significantly weakened, and the peaks in SIP and SFC almost disappeared. Meanwhile, the peaks of Fe_3O_4 were newly detected in SIP and the intensity was slightly increased in SFC. The results provided direct evidence for the corrosion of Fe^0 and the formation of iron oxides on Fe^0 surface, and it confirmed that the corrosion rate of SIP was faster than SIS. Moreover, the change from Fe^0 to Fe_3O_4 occurred in SFC was mainly associated with the tightly adhered corrosion products layer on SFC surface, which could block the releasing of Fe^{2+} and electron, leading to the relatively low TOC and chroma removal efficiency (Yang et al. 2017a).

Figure 4b displayed the XRD analysis of AC surfaces before and after micro-electrolysis treatment. The fresh AC exhibited two broad peaks at around 25° and 43° corresponded to the interlayer reflection of amorphous carbon (Xu et al. 2018a; Yuan et al. 2018). After micro-electrolysis treatment, the intensity of the two broad peaks generally weakened and even disappeared in SIPA system, indicating that plenty of corrosion products adhered to AC surface and disguised the characteristics of AC (Zhu et al. 2018a). And the lower intensity of AC treated by SIPA was related to its quick iron corrosion rate due to the relatively favorable physicochemical properties of SIP.

UV-vis spectral

The UV-vis absorption spectra of the aqueous solution during treatment processes by SIPA, SISA, and SFC under the optimal conditions were shown in Fig. 5. With regard to the UV-vis spectrum of the textile wastewater, a broad peak between 200 and 325 nm was detected. The absorbance peaks near 227 nm could be assigned to the π-π* transition of benzene ring of monoaromatics and small molecules, such as ketones, aldehydes, esters, and aliphatic acids (Wen et al. 2018; Yuan et al. 2016; Zhao et al. 2010). The other two weak peaks observed at 268 nm and 310 nm were ascribed to the benzene

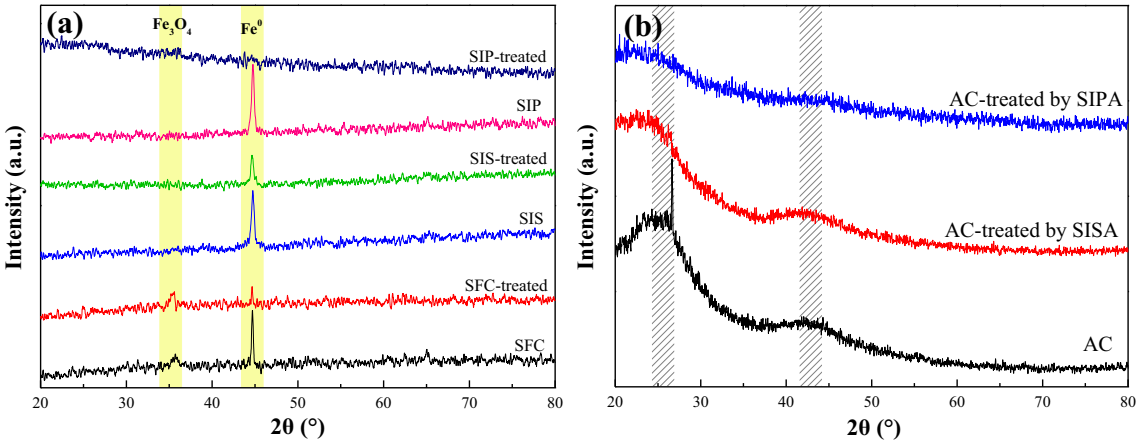

Fig. 4 XRD analysis of fresh and treated electrode materials: **a** SIP, SIS and SFC and **b** AC

rings and naphthalene rings (Wen et al. 2018; Zhu et al. 2018a).

As shown in Fig. 5a, the absorbance peaks of the aqueous solution gradually declined with the time of SIPA treatment. The absorbance peaks at approximately 227 nm dramatically decreased, and the absorbance peaks between 250 and 325 nm were almost disappeared. The result obviously revealed that SIPA could effectively reduce the pollutants by degrading the complex organic compounds into small molecules, and then the small molecules could be continuously removed via oxidation. However, the benzene and naphthalene structure of the pollutants was still hardly to be decomposed. Figure 5b revealed a slightly weakened reduction of the total absorbance peaks in SISA, owing to the relatively less reaction sites. Remarkably, Fig. 5c showed that the total absorbance peaks of the aqueous solution were sharply decreased in the initial

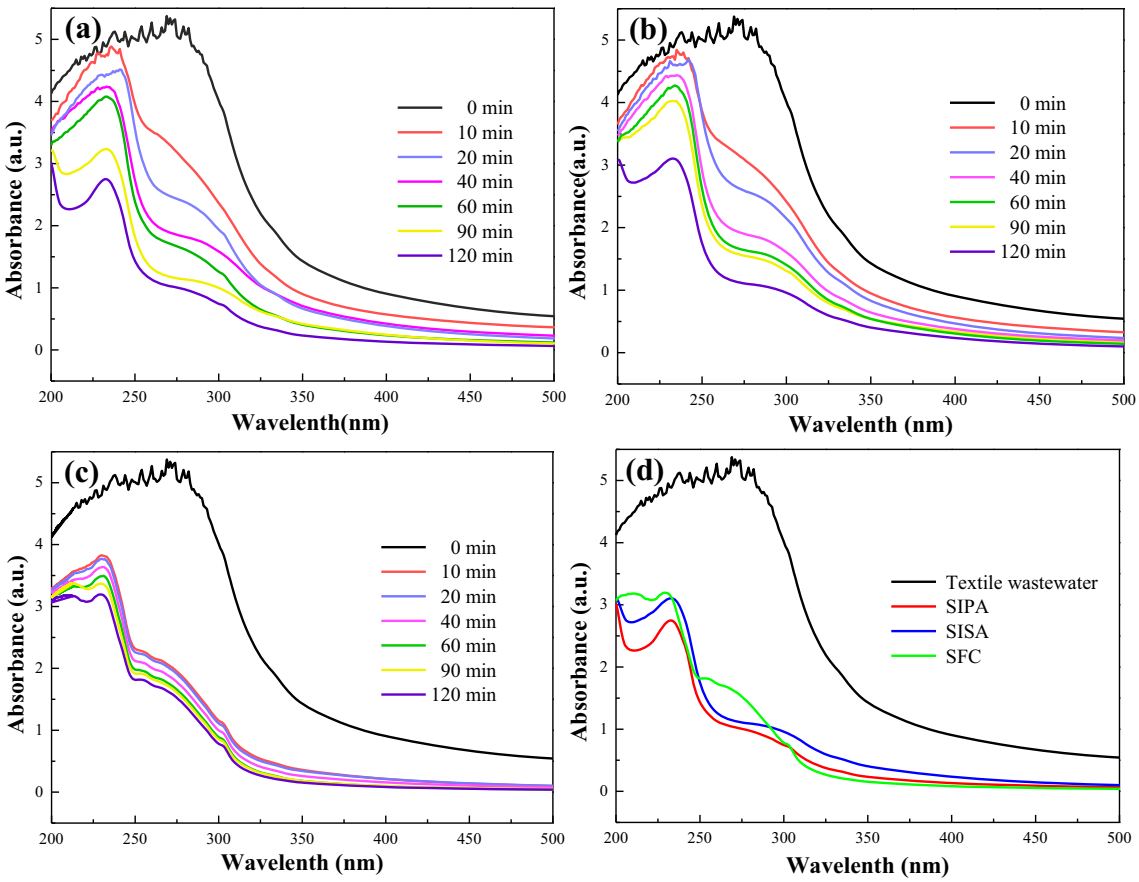

Fig. 5 Time course variations of UV-vis spectra in different systems: **a** SIPA, **b** SISA and **c** SFC, **d** UV-vis spectra of the effluent after 120 min in different systems

10 min, while it changed slowly as the SFC treatment continued in rest of the time. This phenomenon could be reasonably attributed to the rapid adsorption process of pollutants because of the porous structure of SFC. For a better comparison between the treatment capacity of SIPA, SISA, and SFC, the UV-vis spectra of the aqueous solution after 120 min treatment was depicted in Fig. 5d. Not surprisingly, SIPA presented the highest treatment efficiency of the pollutants in textile wastewater, then SISA, and finally SFC.

3DEEM fluorescence

Three-dimensional excitation-emission matrix (3DEEM) fluorescence spectroscopy is a rapid and sensitive technique to analyze dissolved organic matter in wastewater. The 3DEEM spectra for the textile wastewater before and after different micro-electrolysis treatments were shown in Fig. 6. In general, there were three conspicuous fluorescence peaks observed in all 3DEEM spectra. Peak A located at Ex/Em = 275 nm/350 nm, which was associated with soluble microbial product-like substances (Bai et al. 2017). Peak B located at Ex/Em = 230 nm/365 nm was classified as aromatic protein-like substances (Wen et al. 2003). Peak C was related to fulvic acid-like, situated at Ex/Em = 250 nm/455 nm (Bu et al. 2010). According to Fig. 6b and c, the total fluorescence intensity dramatically dropped after SIPA and SISA treatment. In contrast, SFC showed weak effect on the decrease of fluorescence intensity in Fig. 6d. For textile wastewater, the fluorescence peaks mainly derived from the chromophore and auxochrome in dye molecules and intermediates (Langhals and Jona 1998). The decline of the total fluorescence intensity illustrated that the breakage of chromophore and auxochrome and therefore the dyes were degraded into smaller molecules with less weight. In other words, the SIPA and SISA were more effective than the SFC for organic pollutants degradation in actual textile wastewater.

Degradation pathway

To further expound the degradation pathways of textile wastewater in Fe-C micro-electrolysis systems, GC-MS was used to examine the pollutants and intermediates in wastewater before and after different micro-electrolysis treatments. The complex

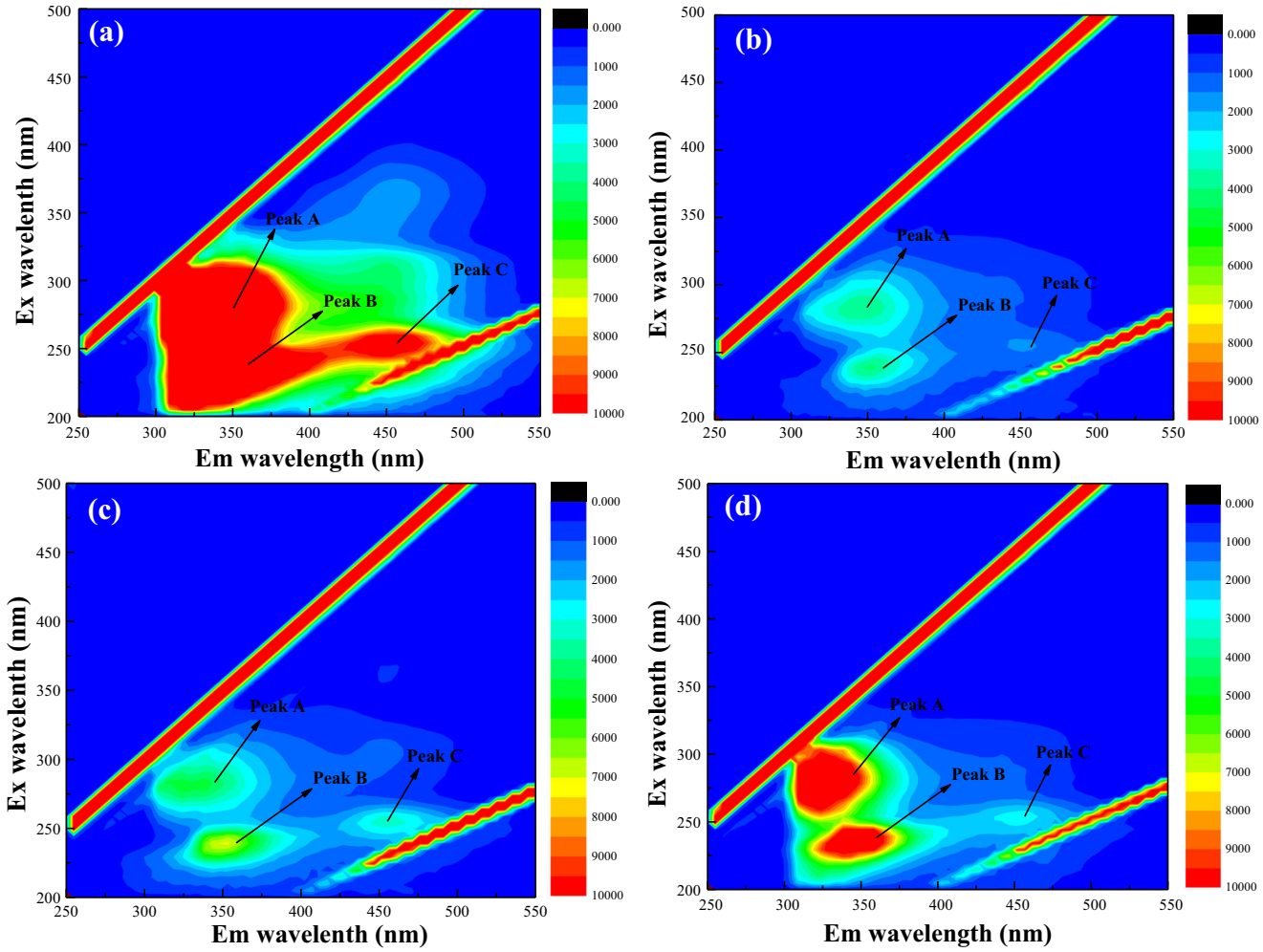

Fig. 6 3DEEM fluorescence spectra of **a** textile wastewater and the effluent after 120 min in different systems: **b** SIPA, **c** SISA, and **d** SFC

and diverse organic pollutants and intermediate species in wastewater were shown in Fig. 7. Here, the variations in the number of main organic pollutant species identified with MW < 518 g/mol and relative peak areas > 0.1% by GC-MS were listed in Table 2. As can be seen, a total of 18 main organic pollutant species were detected in the actual textile wastewater, which were the major contributor to TOC and chroma. After different micro-electrolysis treatments for 120 min, the total number of main organic pollutant species decreased to 11, 13, and 13, respectively. Specifically, 11 main organic pollutant species were totally removed and 4 newly generated after treated by SIPA, while for SISA and SFC, only 7 main organic pollutant species were totally removed and 2 newly generated. The above results demonstrated that the TOC and chroma of textile wastewater could be effectively removed owing to the degradation and abatement of organic pollutants in micro-electrolysis treatment. In addition, SIPA exhibited the most positive effect on the organic pollutants degradation therefore promoting the new generation of intermediates.

The details of the main organic pollutants and intermediate species were enumerated in Table 3. Obviously, the total peak area of main pollutants in SFC was apparently higher than SIPA and SISA. This phenomenon demonstrated that the micro-electrolysis system properly composed of scrap iron and AC exhibited much better treatment capacity for textile wastewater than SFC. In terms of untreated textile wastewater, 18 main organic pollutants could be divided into dyes (Nos. 3, 4, and 5), dye intermediates (No. 12), textile auxiliaries (Nos. 1, 2, 6, 10, 11, 14, and 16), surfactant (Nos. 13 and 15) and other industrial chemicals (Nos. 7, 8, 9, 17, and 18). It was

Table 2 Variations in the number of main organic pollutant species detected by GC-MS before and after different micro-electrolysis treatments

Type of wastewater	Number of main organic pollutant species		
	Total	Totally removed	Newly generated
Textile wastewater	18	/	/
SIPA	11	11	4
SISA	13	7	2
SFC	13	7	2

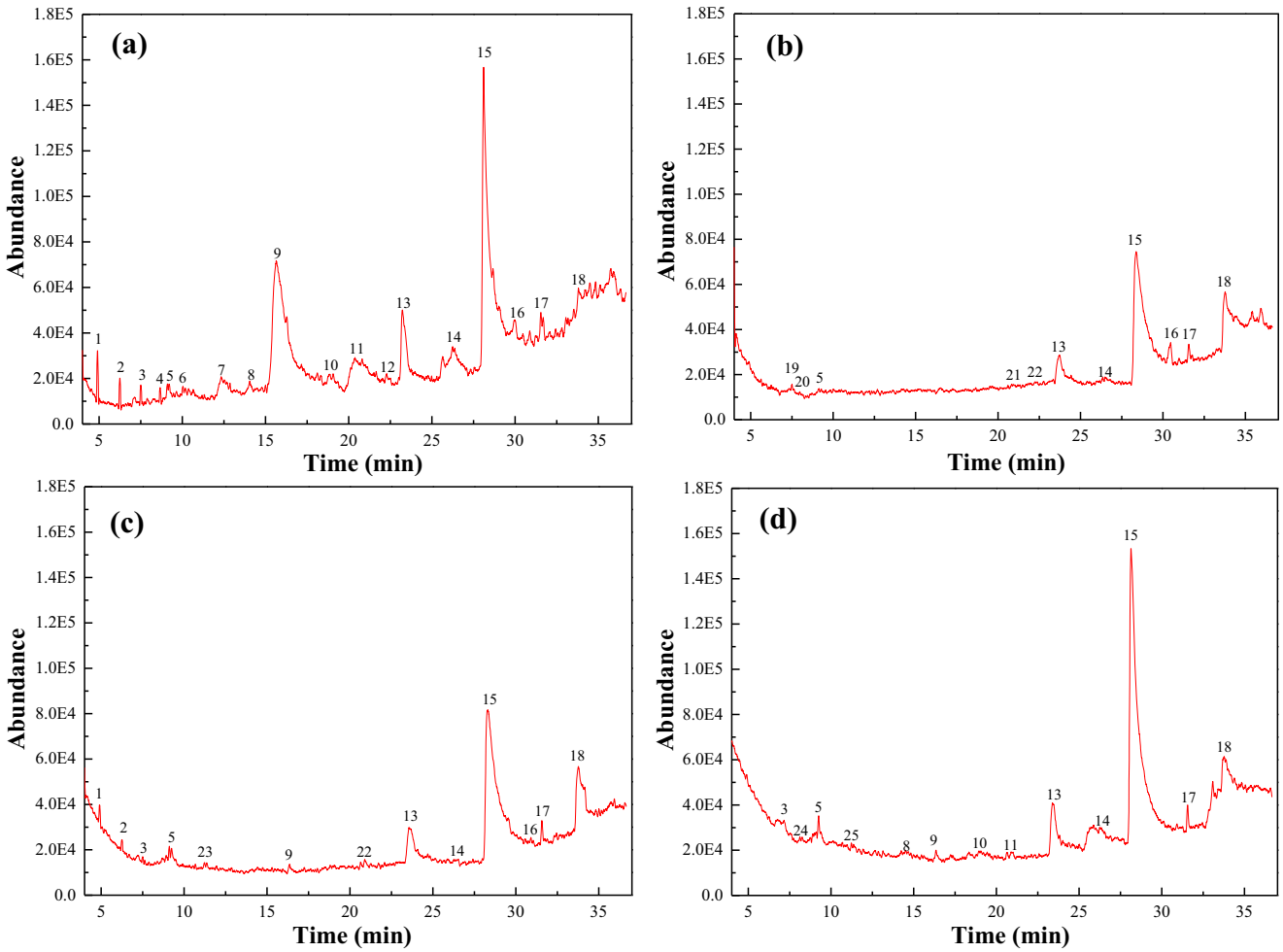

Fig. 7 GC-MS analysis of **a** textile wastewater and the effluent after 120 min in different systems: **b** SIPA, **c** SISA, and **d** SFC

Table 3 Main organic pollutant species detected by GC-MS before and after different micro-electrolysis treatments

No	Organic compounds	Category	MW (g/mol)	Peak Area ($\times 10^7$)			
	Full name			Textile wastewater	SIPA	SISA	SFC
1	Cyclohexasiloxane, dodecamethyl-	TA[a]	444	0.0824	ND[d]	0.0423	ND
2	Cycloheptasiloxane, tetradecamethyl-	TA	518	0.0439	ND	0.0236	ND
3	4-Allyloxy-2-chloroquinazoline	Dye	220	0.0273	ND	0.0172	0.0169
4	Pterin-6-carboxylic acid	Dye	207	0.0197	ND	ND	ND
5	3-Butenamide	Dye	85	0.0318	0.0064	0.0305	0.0182
6	Dihydroxymaleic acid	TA	148	0.0206	ND	ND	ND
7	Tridecanoic acid	OIC[b]	214	0.3174	ND	ND	ND
8	n-Hexadecanoic acid	OIC	256	0.1181	ND	ND	0.0102
9	Octadecanoic acid	OIC	284	1.1173	ND	0.0388	0.0430
10	1,2-Benzenedicarboxylic acid, bis(2-methylpropyl) ester	TA	278	0.0281	ND	ND	0.0246
11	2-Chloropropionic acid, octadecyl ester	TA	360	0.4351	ND	ND	0.0304
12	3,3′-Iminobispropylamine	DI[c]	131	0.0387	ND	ND	ND
13	Octadecanamide	Surfactant	283	0.5559	0.3015	0.3259	0.3893
14	2-Dimethylaminomethyl-4-chloro-1-naphthol	TA	235	0.1060	0.0168	0.0915	0.0614
15	Oleamide	Surfactant	281	2.5532	1.6679	1.7854	2.3870
16	2H-1,4-Benzoxazin-3(4H)-one	TA	149	0.0401	0.0310	0.0160	ND
17	Sarcosine, N-(cyclohexylcarbonyl)-, butyl ester	OIC	255	0.0507	0.0808	0.0566	0.0658
18	Sarcosine, N-(cyclohexylcarbonyl)-, tetradecyl ester	OIC	395	0.5903	0.1133	0.2350	0.2643
19	Glycidol	OIC	74	ND	0.0129	ND	ND
20	Ethyl hydrogen oxalate	DI	118	ND	0.0105	ND	ND
21	3-Chloro-N-methylpropylamine	OIC	107	ND	0.0160	ND	ND
22	Acetamide	OIC	59	ND	0.0206	0.0413	ND
23	Cyclopropyl carbinol	OIC	72	ND	ND	0.0165	ND
24	Dodecane	OIC	170	ND	ND	ND	0.0092
25	2-Chloro-4,6-dimethylquinoline	DI	191	ND	ND	ND	0.0085

[a] *TA*, textile auxiliaries

[b] *OIC*, other industrial chemicals

[c] *DI*, dye intermediates

[d] *ND*, not detected

obvious that most pollutants were degraded into smaller molecules with lower weight after different micro-electrolysis treatments. Above discoveries directly supported the TOC removal of textile wastewater. Especially, massive aliphatic acids (Nos. 8 and 9) were almost completely removed, showing the disappearance of corresponding GC-MS peaks in Fig. 7. Meanwhile, excellent removal efficiency of chroma obtained by virtue of the decomposition of dyes by micro-electrolysis treatments. Nevertheless, the amides were hard to be degraded by micro-electrolysis, leading to the TOC residual in effluent (Qin et al. 2016).

Figure 8 proposed the possible degradation pathways of intermediates in textile wastewater treated by different Fe-C micro-electrolysis systems. In terms of newly generated organic species, Fig. 8a showed that 4 newly generated organic species were detected in SIPA. In the presence of [H], glycidol and ethyl hydrogen oxalate might be produced from the hydrogenation reduction of dihydroxymaleic acid and the breakage of branches on benzene ring of 1,2-benzenedicarboxylic acid, bis(2-methylpropyl) ester. Meanwhile, the formation of 3-chloro-N-methylpropylamine might be due to the cracking of 3,3′-iminobispropylamine and benzene ring opening of 2-dimethylaminomethyl-4-chloro-1-naphthol under the attack of ·OH. Moreover, acetamide was probably generated from the amide compounds by the cleavage of carbon chain, but the amide group could hardly be further removed.

Similar degradation pathways in SISA system were presented in Fig. 8b, but less intermediates was generated due to the relatively unfavorable physicochemical properties of SIS. Amide compounds were degraded into acetamide and other small molecules, and cyclopropyl carbinol might be derived from the reduction and reorganization of dihydroxymaleic acid and 1,2-benzenedicarboxylic acid, bis(2-methylpropyl) ester.

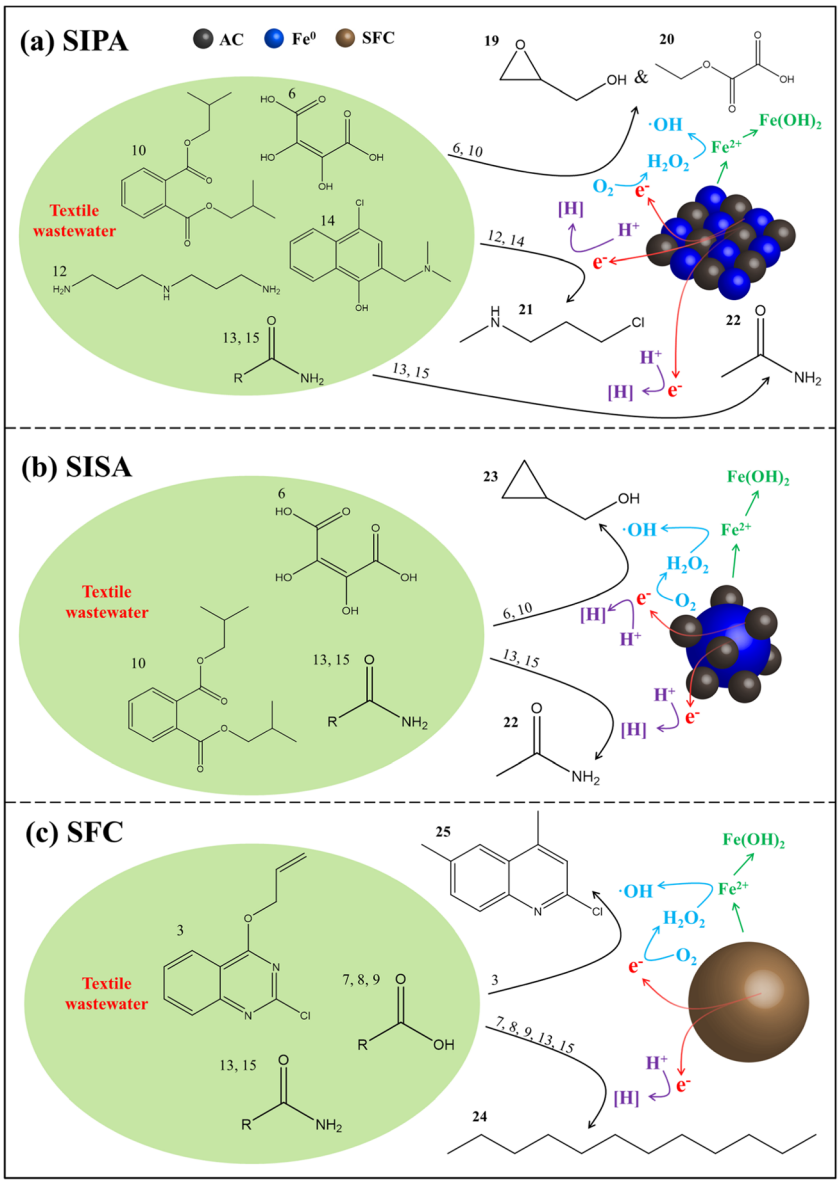

Fig. 8 Degradation pathways of pollutants in textile wastewater treated by different Fe-C micro-electrolysis. The numbers represent the serial number of pollutants listed in the Table 3

It was interesting to find that 2 new organic species generated in SFC were completely different from those in SIPA and SISA (Fig. 8c). Presumably, the generation of dodecane was attributed to the carbon chain breakage and incomplete degradation of aliphatic acids and amides, which could be easily removed by SIPA and SISA. 2-chloro-4,6-dimethylquinoline might be derived from 4-allyloxy-2-chloroquinazoline considering their similar chemical structure, which also revealed the poor ring opening and dechlorination capability of SFC.

Stability of different systems

To investigate the stability of different Fe-C micro-electrolysis systems, 10 consecutive experiments were carried out, as shown in Fig. 9. The TOC and chroma removal efficiency in SIPA and SISA were stable and performed well after the tenth run. The results indicated that the above systems had high stability and excellent reusability, which was probably due to the sustained reactivity of Fe^0 in acidic solution, surface load reduction of Fe^0 in the presence of AC and negligible iron loss (Zhang et al. 2015). While for SFC, owing to its surface passivation, blockage, and mass transport limitation, the TOC removal efficiency decreased from 44.7 to 36.4% after the tenth run, and the corresponding chroma removal efficiency decreased from 76.0 to 67.8%.

Cost analysis

The evaluated costs of SIPA, SISA, and SFC for treating actual textile wastewater included the preparation cost and Fe^0 consumption. Consisting of SIP/SIS (900 CNY/t) and AC (3000 CNY/t) of the equal mass, SIPA and

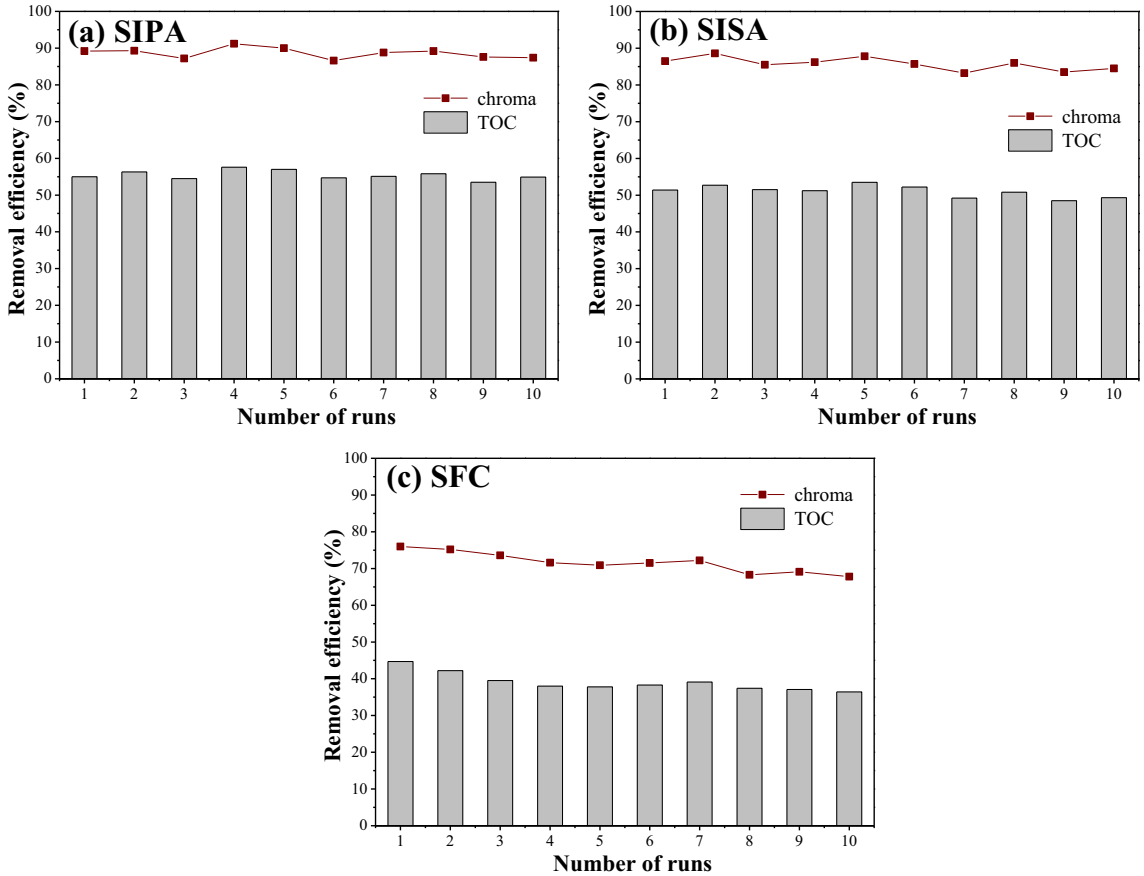

Fig. 9 TOC and chroma removal of SIPA **a**, SISA **b**, and SFC **c** in 10 times consecutive experiments. Experiment conditions: initial pH = 3.0, dosage = 30 g/L, Fe/AC = 1:1, stirring speed = 200 rpm

SISA could both be prepared for only around 1950 CNY/t, which were about 23% of the preparation cost of SFC (8500 CNY/t). Also, about 124 g and 95 g Fe^0 of SIPA and SISA would be consumed per treatment of 1 ton actual textile wastewater. Thus it could be obtained that the corresponding costs of Fe^0 consumption of SIPA and SISA were only 0.24 CNY and 0.18 CNY per treatment of 1 ton actual textile wastewater. As a result, compared with SFC, scrap iron-AC micro-electrolysis was an economical technique to treat actual textile wastewater.

Conclusions

In this study, two types of scrap irons were used as anode materials to establish Fe-C micro-electrolysis systems for actual textile wastewater treatment. The optimal parameters of SIPA and SISA were initial pH of 3.0, dosage of 30 g/L and Fe/C mass ratio of 1:1. The TOC removal efficiencies of SIPA, SISA, and SFC at optimal conditions were 55.0%, 51.4%, and 44.7%, respectively, confirming the superiority of SIPA and SISA. According to the total iron concentration and XRD analysis, the physicochemical properties of scrap iron were found to be a key factor that dominates the formation of microscopic galvanic cell and the iron corrosion intensity. The UV-vis and 3DEEM analysis demonstrated the direct relationship between pollutants degradation and TOC and chroma removals. Furthermore, variations in organic pollutant species including dyes, dye intermediates, textile auxiliaries, and other pollutants were analyzed by GC-MS. More pollutants such as aliphatic acids, amides, dyes, and dye intermediates were removed by the combination of reduction and oxidation in SIPA and SISA than that by SFC. SIPA and SISA possessed better removal efficiency for chlorine and benzene ring than SFC. Besides, SIPA and SISA possessed excellent stability in successive runs. Therefore, scrap iron-AC micro-electrolysis could be considered as a cost-effective, feasible, and promising method for the treatment of actual textile wastewater.

Funding information This work was financially supported by the National Natural Science Foundation of China (21707090), Chinese Postdoctoral Science Foundation (2017M611590), and Shanghai Natural Science Foundation (14ZR1428900).

References

Bai Z, Wang J, Yang Q (2017) Advanced treatment of municipal secondary effluent by catalytic ozonation using Fe_3O_4-CeO_2/MWCNTs as efficient catalyst. Environ Sci Pollut Res 24:9337–9349

Brillas E, Martínez-Huitle CA (2015) Decontamination of wastewaters containing synthetic organic dyes by electrochemical methods. An updated review. Appl Catal B Environ 166-167:603–643

Btatkeu KBD, Miyajima K, Noubactep C, Caré S (2013) Testing the suitability of metallic iron for environmental remediation: discoloration of methylene blue in column studies. Chem Eng J 215-216: 959–968

Bu L, Wang K, Zhao QL, Wei LL, Zhang J, Yang JC (2010) Characterization of dissolved organic matter during landfill leachate treatment by sequencing batch reactor, aeration corrosive cell-Fenton, and granular activated carbon in series. J Hazard Mater 179:1096–1105

Deng J, Dong H, Zhang C, Jiang Z, Cheng Y, Hou K, Zhang L, Fan C (2018) Nanoscale zero-valent iron/biochar composite as an activator for Fenton-like removal of sulfamethazine. Sep Purif Technol 202: 130–137

Dou X, Li R, Zhao B, Liang W (2010) Arsenate removal from water by zero-valent iron/activated carbon galvanic couples. J Hazard Mater 182:108–114

Doumic LI, Soares PA, Ayude MA, Cassanello M, Boaventura RAR, Vilar VJP (2015) Enhancement of a solar photo-Fenton reaction by using ferrioxalate complexes for the treatment of a synthetic cotton-textile dyeing wastewater. Chem Eng J 277:86–96

Eremektar G, Selcuk H, Meric S (2007) Investigation of the relation between COD fractions and the toxicity in a textile finishing industry wastewater: effect of preozonation. Desalination 211:314–320

Gheju M, Balcu I (2010) Hexavalent chromium reduction with scrap iron in continuous-flow system. Part 2: effect of scrap iron shape and size. J Hazard Mater 182:484–493

Guan X, Sun Y, Qin H, Li J, Lo IMC, He D, Dong H (2015) The limitations of applying zero-valent iron technology in contaminants sequestration and the corresponding countermeasures: the development in zero-valent iron technology in the last two decades (1994-2014). Water Res 75:224–248

Han Y, Li H, Liu M, Sang Y, Liang C, Chen J (2016) Purification treatment of dyes wastewater with a novel micro-electrolysis reactor. Sep Purif Technol 170:241–247

Huang D, Yue Q, Fu K, Zhang B, Gao B, Li Q, Wang Y (2014) Application for acrylonitrile wastewater treatment by new micro-electrolysis ceramic fillers. Desalin Water Treat 57:4420–4428

Khandegar V, Saroha AK (2013) Electrocoagulation for the treatment of textile industry effluent–a review. J Environ Manag 128:949–963

Lai B, Zhang Y, Chen Z, Yang P, Zhou Y, Wang J (2014) Removal of p-nitrophenol (PNP) in aqueous solution by the micron-scale iron-copper (Fe/Cu) bimetallic particles. Appl Catal B Environ 144: 816–830

Lai B, Zhou Y, Qin H, Wu C, Pang C, Lian Y, Xu J (2012) Pretreatment of wastewater from acrylonitrile-butadiene-styrene (ABS) resin manufacturing by microelectrolysis. Chem Eng J 179:1–7

Lai B, Zhou Y, Yang P, Yang J, Wang J (2013) Degradation of 3,3′-iminobis-propanenitrile in aqueous solution by Fe^0/GAC micro-electrolysis system. Chemosphere 90:1470–1477

Langhals H, Jona W (1998) Intense dyes through chromophore-chromophore interactions: bi- and trichromophoric perylene-3,4:9, 10-bis(dicarboximide)s. Angew Chem Int Ed 37:952–955

Li C, Wang H, Lu D, Wu W, Ding J, Zhao X, Xiong R, Yang M, Wu P, Chen F, Fang P (2017) Visible-light-driven water splitting from dyeing wastewater using Pt surface-dispersed TiO_2-based nanosheets. J Alloys Compd 699:183–192

Liu H, Li G, Qu J, Liu H (2007) Degradation of azo dye acid Orange 7 in water by Fe^0/granular activated carbon system in the presence of ultrasound. J Hazard Mater 144:180–186

Liu P, Keller J, Gernjak W (2016) Enhancing zero valent iron based natural organic matter removal by mixing with dispersed carbon cathodes. Sci Total Environ 550:95–102

Luo J, Song G, Liu J, Qian G, Xu ZP (2014) Mechanism of enhanced nitrate reduction via micro-electrolysis at the powdered zero-valent iron/activated carbon interface. J Colloid Interface Sci 435:21–25

Manu B, Chaudhari S (2002) Anaerobic decolorisation of simulated textile wastewater containing azo dyes. Bioresour Technol 82:225–231

Ou C, Shen J, Zhang S, Mu Y, Han W, Sun X, Li J, Wang L (2016) Coupling of iron shavings into the anaerobic system for enhanced 2,4-dinitroanisole reduction in wastewater. Water Res 101:457–466

Qin L, Zhang G, Meng Q, Xu L, Lv B (2012) Enhanced MBR by internal micro-electrolysis for degradation of anthraquinone dye wastewater. Chem Eng J 210:575–584

Qin Z, Liu S, Liang S-x, Kang Q, Wang J, Zhao C (2016) Advanced treatment of pharmaceutical wastewater with combined micro-electrolysis, Fenton oxidation, and coagulation sedimentation method. Desalin Water Treat 57:25369–25378

Regti A, Ben El Ayouchia H, Laamari MR, Stiriba SE, Anane H, El Haddad M (2016) Experimental and theoretical study using DFT method for the competitive adsorption of two cationic dyes from wastewaters. Appl Surf Sci 390:311–319

Ruan X-C, Liu M-Y, Zeng Q-F, Ding Y-H (2010) Degradation and decolorization of reactive red X-3B aqueous solution by ozone integrated with internal micro-electrolysis. Sep Purif Technol 74:195–201

Sun L, Song H, Li Q, Li A (2016) Fe/Cu bimetallic catalysis for reductive degradation of nitrobenzene under toxic conditions. Chem Eng J 283:366–374

Van der Zee FP, Bisschops IAE, Lettinga G, Field JA (2003) Activated carbon as an electron acceptor and redox mediator during the anaerobic biotransformation of azo dyes. Environ Sci Technol 37:402–408

Wen C, Paul W, Leenheer JA, Karl B (2003) Fluorescence excitation-emission matrix regional integration to quantify spectra for dissolved organic matter. Environ Sci Technol 37:5701–5710

Wen C, Xu X, Fan Y, Xiao C, Ma C (2018) Pretreatment of water-based seed coating wastewater by combined coagulation and sponge-iron-catalyzed ozonation technology. Chemosphere 206:238–247

Xu X, Cheng Y, Zhang T, Ji F, Xu X (2016) Treatment of pharmaceutical wastewater using interior micro-electrolysis/Fenton oxidation-coagulation and biological degradation. Chemosphere 152:23–30

Xu Z, Tian D, Sun Z, Zhang D, Zhou Y, Chen W, Deng H (2019) Highly porous activated carbon synthesized by pyrolysis of polyester fabric wastes with different iron salts: pore development and adsorption behavior. Colloids Surf A Physicochem Eng Asp 565:180–187

Xu Z, Yuan Z, Zhang D, Chen W, Huang Y, Zhang T, Tian D, Deng H, Zhou Y, Sun Z (2018a) Highly mesoporous activated carbon synthesized by pyrolysis of waste polyester textiles and $MgCl_2$: physiochemical characteristics and pore-forming mechanism. J Clean Prod 192:453–461

Xu Z, Zhang T, Yuan Z, Zhang D, Sun Z, Huang YX, Chen W, Tian D, Deng H, Zhou Y (2018b) Fabrication of cotton textile waste-based magnetic activated carbon using $FeCl_3$ activation by the Box-Behnken design: optimization and characteristics. RSC Adv 8: 38081–38090

Ya V, Guillou EL, Chen YM, Yu JH, Choo KH, Chuang SM, Lee SJ, Li CW (2018) Scrap iron packed in a Ti mesh cage as a sacrificial anode for electrochemical Cr(VI) reduction to treat electroplating wastewater. J Taiwan Inst Chem Eng 87:91–97

Yahiaoui I, Aissani-Benissad F, Madi K, Benmehdi N, Fourcade F, Amrane A (2013) Electrochemical pre-treatment combined with biological treatment for the degradation of methylene blue dye: Pb/

PbO_2 electrode and modeling-optimization through central composite design. Ind Eng Chem Res 52:14743–14751

Yamaguchi R, Kurosu S, Suzuki M, Kawase Y (2018) Hydroxyl radical generation by zero-valent iron/Cu (ZVI/Cu) bimetallic catalyst in wastewater treatment: heterogeneous Fenton/Fenton-like reactions by Fenton reagents formed in-situ under oxic conditions. Chem Eng J 334:1537–1549

Yang K, Jin Y, Yue Q, Zhao P, Gao Y, Wu S (2017a) Comparison of two modified coal ash ferric-carbon micro-electrolysis ceramic media for pretreatment of tetracycline wastewater. Environ Sci Pollut Res 24: 12462–12473

Yang Z, Ma Y, Liu Y, Li Q, Zhou Z, Ren Z (2017b) Degradation of organic pollutants in near-neutral pH solution by Fe-C micro-electrolysis system. Chem Eng J 315:403–414

Ying D, Xu X, Li K, Wang Y, Jia J (2012) Design of a novel sequencing batch internal micro-electrolysis reactor for treating mature landfill leachate. Chem Eng Res Des 90:2278–2286

Yuan L, Zhi W, Xie Q, Chen X, Liu Y (2015) Lead removal from solution by a porous ceramisite made from bentonite, metallic iron, and activated carbon. Environ Sci 1:814–822

Yuan Y, Lai B, Tang Y-Y (2016) Combined Fe^0/air and Fenton process for the treatment of dinitrodiazophenol (DDNP) industry wastewater. Chem Eng J 283:1514–1521

Yuan Z, Xu Z, Zhang D, Chen W, Zhang T, Huang Y, Gu L, Deng H, Tian D (2018) Box-Behnken design approach towards optimization of activated carbon synthesized by co-pyrolysis of waste polyester textiles and $MgCl_2$. Appl Surf Sci 427:340–348

Zhang C, Zhou M, Yu X, Ma L, Yu F (2015) Modified iron-carbon as heterogeneous electro-Fenton catalyst for organic pollutant degradation in near neutral pH condition: characterization, degradation activity and stability. Electrochim Acta 160:254–262

Zhang Y, Yang B, Han Y, Jiang C, Wu D, Fan J, Ma L (2016) Novel iron metal matrix composite reinforced by quartz sand for the effective dechlorination of aqueous 2-chlorophenol. Chemosphere 146:308–314

Zhao S, Ma H, Wang M, Cao C, Xiong J, Xu Y, Yao S (2010) Study on the mechanism of photo-degradation of p-nitrophenol exposed to 254 nm UV light. J Hazard Mater 180:86–90

Zhou H, Lv P, Shen Y, Wang J, Fan J (2013) Identification of degradation products of ionic liquids in an ultrasound assisted zero-valent iron activated carbon micro-electrolysis system and their degradation mechanism. Water Res 47:3514–3522

Zhu F, Ma S, Liu T, Deng X (2018b) Green synthesis of nano zero-valent iron/cu by green tea to remove hexavalent chromium from groundwater. J Clean Prod 174:184–190

Zhu X, Chen X, Yang Z, Liu Y, Zhou Z, Ren Z (2018a) Investigating the influences of electrode material property on degradation behavior of organic wastewaters by iron-carbon micro-electrolysis. Chem Eng J 338:46–54